Hyperfine Interactions 123/124 (1999) 427–454

Nuclear resonant scattering of synchrotron radiation by multilayer structures

A.I. Chumakov [a,*], L. Niesen [b], D.L. Nagy [c] and E.E. Alp [d]

[a] *European Synchrotron Radiation Facility, BP 220, F-38043 Grenoble, France*
E-mail: chumakov@esrf.fr
[b] *Nuclear Solid State Physics, Materials Science Center, Groningen University, Nijenborgh 4, 9747 AG Groningen, The Netherlands*
[c] *KFKI Research Institute for Particle and Nuclear Physics, P.O.B. 49, H-1525 Budapest, Hungary*
[d] *Advanced Photon Source, Argonne National Laboratory, Argonne, IL 60439, USA*

Multilayer structures form a particular class of samples employed in nuclear resonant scattering of synchrotron radiation. Their specific properties lead to unusual energy and time characteristics of nuclear resonant scattering, which differ much from those of single crystals. The analysis of these distinctions is presented. Several approaches to achieve pure nuclear reflections with multilayers are discussed. Finally, we review the studies of multilayer structures with nuclear resonant scattering of synchrotron radiation.

1. Introduction

Since the challenge to excite nuclei by synchrotron radiation has been formulated, multilayer structures were suggested as a promising tool to filter narrow resonant X-ray components from the broad-band energy spectrum of synchrotron radiation [1]. The original idea was as simple as it was effective: a multilayer composed of layers of different isotopes of the same element possesses the periodicity only of the nuclear density but not the electronic one. If one of the isotopes has an appropriate nuclear resonant transition, this structure should work as a periodic multilayer for the radiation in the vicinity of the nuclear resonance, whereas it should act like a homogeneous sample for the radiation far off the resonance. In particular, the Bragg reflections of this periodic multilayer should contain only the nuclear resonant components of synchrotron radiation.

The filtering application was the main motivation in early studies of nuclear resonant scattering by multilayers. A nuclear resonant monochromator of synchrotron radiation on the basis of a periodic multilayer allows a wide latitude of design. In contrast to single crystals, where all scattering features are rigidly defined by nature, with artificial multilayer structures one can freely choose almost every parameter of scattering including the resonant energy, hyperfine structure, Bragg angle, and the

[*] Also at Russian Research Center Kurchatov Institute, 123182 Moscow, Russia.

angular width of the reflection. The optimization of the parameters for the highest nuclear reflectivity and the largest suppression of nonresonant electronic scattering was performed in computer simulations [2–6]. The required theory of nuclear scattering by layered structures was developed on the basis of the conventional optical Fresnel formalism and the recursive Parratt routine [7], which were adapted to the energy-dispersive case of resonant scattering [8,9]. Several nuclear resonant monochromators of synchrotron radiation on the basis of periodic multilayers were developed and examined with nuclear γ-radiation of Mössbauer sources [10–12] and with synchrotron radiation [13,14]. The goal of pure nuclear scattering was achieved: the devices showed sufficiently high reflectivity of resonant radiation in the vicinity of nuclear transition and good rejection of the nonresonant electronic scattering.

Already the first synchrotron radiation experiments with resonant multilayers showed the tremendous potential providing both structural and spectroscopic information on these systems. By combining time-domain hyperfine nuclear spectroscopy with grazing-angle X-ray scattering, a powerful technique to investigate layered structures was established. The coherent nature of scattering provides the basis for the site-selective hyperfine nuclear spectroscopy [14]. This option was further developed with the technique of selective deposition of the resonant isotope, where sensitivity of nuclear scattering to one single monolayer of the resonant atoms was achieved [15]. Moreover, the strong angular dependence of the penetration depth of X-rays in the vicinity of total reflection was used for depth-selective hyperfine nuclear spectroscopy [16].

Finally, nuclear multilayers gave a new impact to understanding the physics of coherent nuclear resonant scattering. Similarly to single crystals, they supplied a tool to study the nuclear resonant diffraction of X-rays. However, the quite different scattering parameters (long spatial periodicity, small number of reflecting planes, low structure factors) drastically change the properties of nuclear diffraction.

In this paper we analyze the special features of nuclear resonant scattering of synchrotron radiation by multilayer structures, discuss various approaches to suppress the electronic channel of X-ray scattering, and give a review of the experimental investigations of nuclear resonant multilayers using synchrotron radiation.

2. Special features of nuclear resonant scattering of X-rays by periodic multilayers

The physics of nuclear resonant scattering of synchrotron radiation by periodic multilayers is similar to that of single crystals [17]. In general, both cases can be treated with the same dynamical theory of X-ray diffraction, which takes into account the specular reflected beam [18] and the optical activity of the medium. However, several features of periodic multilayers lead to special cases, which are not typical for single crystals.

First, the number of reflecting planes in a periodic multilayer is small. This results in large angular widths of the reflections. In addition, this leads, in terms of the diffraction theory, to the two wave-field case of Bragg diffraction in a thin sample.

Second, the spatial period of a multilayer is by an order of magnitude larger than the lattice constant of crystals. Therefore the Bragg angles are small, typically only a few times larger than the critical angle of total reflection. This implies significant refraction effects.

Finally, the resonant nuclei do not occupy discrete positions in the unit cell, but are, as a rule, distributed over a significant part of the period. Therefore the structure factor of the Bragg reflection is always smaller than unity. This means that, in contrast to single crystals, a complete suppression of inelastic channels of nuclear resonant scattering [19–22] can never be achieved in the case of multilayers. Therefore, scattering cannot compete with absorption as efficiently as it does in the case of single crystals.

Below, we shall consider how these distinctions influence the nuclear resonant scattering of X-rays by periodic multilayers. We illustrate the analysis by computer simulations of the properties of the model nuclear periodic multilayers $[^{57}\mathrm{Fe}(d_{57})/^{56}\mathrm{Fe}(d_{56})]\cdot N$ on a glass substrate. Here d_{57} and d_{56} (in Å) stand for the thickness of the layer made out of ^{57}Fe or ^{56}Fe isotopes, respectively, and N is the number of periods. We assume a single line nuclear transition and the absence of inhomogeneous broadening. The simulations were performed with a computer code utilizing the conventional Fresnel–Parratt recursive routine [7], adapted for the energy-dispersive case of nuclear resonant scattering.

Figure 1 shows the angular dependence of nuclear and electronic reflectivity for a $[^{57}\mathrm{Fe}(10)/^{56}\mathrm{Fe}(30)]\cdot 25$ multilayer. We define nuclear reflectivity as the intensity of scattering, integrated over time after excitation and normalized to the number of quanta of incident radiation in the energy interval of one natural width Γ_0 of nuclear transition. The electronic reflectivity has a region of total external reflection below the critical angle of 3.83 mrad. At higher angles Kiessig beats [23] are seen, which originate from the interference of the waves scattered by the top and the bottom boundaries of the multilayer. The period of these beats is $\Delta\theta_K = \lambda/2D = 0.43$ mrad, where $\lambda = 0.86$ Å is the wavelength of the 14.4 keV resonant radiation; $D = Nd_0$ is the total thickness of the structure, and $d_0 = (d_{57} + d_{56})$ is the spatial period. The electronic reflectivity has no Bragg peak since there is no periodicity in the electronic density. The nuclear reflectivity does not have a plateau of total external reflection but a peak at the position of the critical angle [6,24]. Similarly to the electronic reflectivity, the nuclear reflectivity also exhibits Kiessig beats. Moreover, the nuclear reflectivity shows a peak of Bragg reflection in accordance with the periodicity of nuclear density. The Bragg angle θ_B for the m-order reflection may be approximated as

$$\theta_\mathrm{B} \approx \sqrt{(\theta_\mathrm{C})^2 + \left(\frac{m\lambda}{2d_0}\right)^2}, \tag{2.1}$$

where $\theta_\mathrm{C} = \sqrt{-\mathrm{Re}(\tilde{\chi})}$ is the critical angle of specular reflection, $\tilde{\chi}$ is the complex susceptibility (half of the complex increment $\tilde{\delta}$ of the refraction index),

$$\tilde{\chi} = \tilde{\chi}' + \mathrm{i}\tilde{\chi}'' = -\frac{\lambda^2 r_0}{\pi} n\left[Z + \Delta f' - \mathrm{i}\Delta f''\right], \tag{2.2}$$

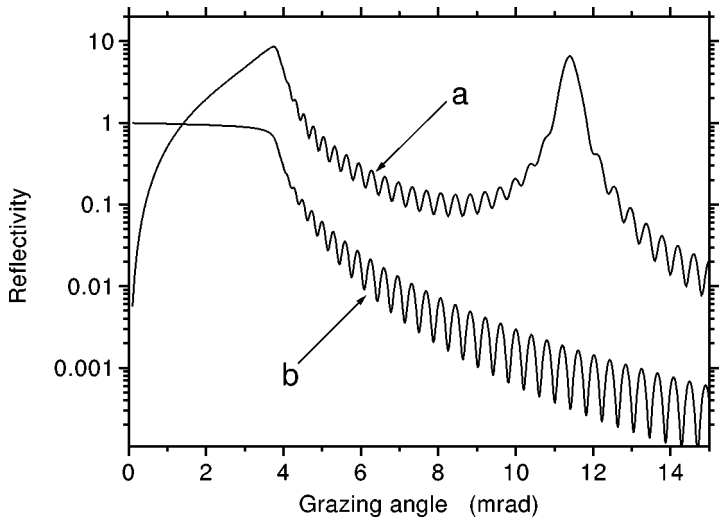

Figure 1. Computer simulation of (a) nuclear and (b) electronic reflectivity for a $[^{57}\mathrm{Fe}(10)/^{56}\mathrm{Fe}(30)] \cdot 25$ multilayer as a function of the grazing angle. Here and below the electronic reflectivity is normalized to the total intensity of the incident beam, whereas the nuclear reflectivity is normalized to the intensity of the incident beam in the energy interval of one natural linewidth of nuclear transition. For this and further simulation the product of the Lamb–Mössbauer factor and the isotope abundance is taken $f_{\mathrm{LM}}\eta = 0.34$.

r_0 is the classical electron radius, n is the atomic density, Z is the atomic number, and $\Delta f' - \mathrm{i}\Delta f''$ is the complex dispersion correction to the atomic scattering factor. The shift of the Bragg angle $\theta_{\mathrm{B}} = 11.41$ mrad (figure 1) from the kinematical value of $\lambda/2d_0 = 10.75$ mrad is determined by refraction of the radiation at the top boundary of the multilayer.

2.1. Angular width of reflections

The angular width of the first-order nuclear reflection in figure 1 is about 0.45 mrad, which is close to one period of the Kiessig beats $\Delta\theta_{\mathrm{K}} = 0.43$ mrad. This is not just a coincidence, since both values are defined by the same kinematical reasoning. The angular dependence of nuclear resonant diffraction of synchrotron radiation comprises angular dependencies of many spectral components. The shape of the rocking curve for each particular component depends on its energy shift from nuclear resonance [25]. The components in close vicinity to the resonance have large scattering amplitudes. This provides high reflectivity and results in some dynamical effects. In particular, the width of reflection scales with the amplitude of nuclear scattering. In contrast, scattering of radiation far away from resonance proceeds kinematically. In this energy region reflectivity is smaller, and the width of reflection is determined merely by an effective number of reflecting planes. The overall angular dependence of nuclear scattering of synchrotron radiation results from averaging of rocking curves of all spectral components. Resonant components contribute with high reflectivity, but this energy region is relatively small. Off-resonant components contribute with smaller

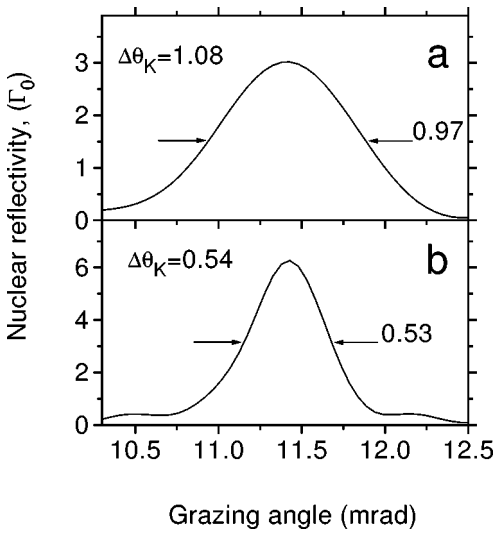

Figure 2. Computer simulation of the angular dependence of the first-order nuclear Bragg reflection for a $[^{57}\mathrm{Fe}(15)/^{56}\mathrm{Fe}(25)] \cdot N$ multilayer with number of periods (a) $N = 10$ and (b) $N = 20$. Note the good agreement of the indicated Kiessig beat period $\Delta\theta_\mathrm{K}$ with the actual width of the reflection.

reflectivity, but this contribution is collected over a larger energy region. Numerical calculations show that the width of nuclear Bragg reflection of synchrotron radiation (both for multilayers and single crystals) is mainly determined by kinematical scattering of the off-resonant components. In most cases the width of the reflection is given merely by the effective number of reflecting planes as $\Delta\theta \approx \lambda/2d_0N \approx \theta_\mathrm{B}/N$ and does not depend on the nuclear scattering amplitude. Figure 2 shows the angular dependence of nuclear reflectivity for a $[^{57}\mathrm{Fe}(15)/^{56}\mathrm{Fe}(25)] \cdot N$ multilayer with number of periods (a) $N = 10$ and (b) $N = 20$. The larger number of reflecting planes results in a narrower width of the reflection. Note that one period of the Kiessig beats $\Delta\theta_\mathrm{K} \approx \theta_\mathrm{B}/N$ gives a good approximation of the angular width for both cases.

For typical parameters of a periodic multilayer $\theta_\mathrm{B} = 10$ mrad and $N \leqslant 100$ we have $\Delta\theta \geqslant 100$ μrad. Therefore the typical angular width of a nuclear reflection for a periodic multilayer is by an order of magnitude larger than the angular divergence of synchrotron radiation. Even for multilayers with a large number of periods the angular width of the reflections remains large because the effective number of reflecting planes is limited by the small penetration depth of X-rays at small grazing angles.

2.2. Energy dispersive refraction

The large angular width of the reflections permits almost ideal angle-resolved conditions of nuclear diffraction. Therefore several angle-dependent effects, which may be observed in single crystals only with an extreme collimation of X-ray beams [25–28], become common features in the case of multilayers. An example is the energy-dependent refraction. Figure 3 shows the energy spectra of nuclear resonant diffraction

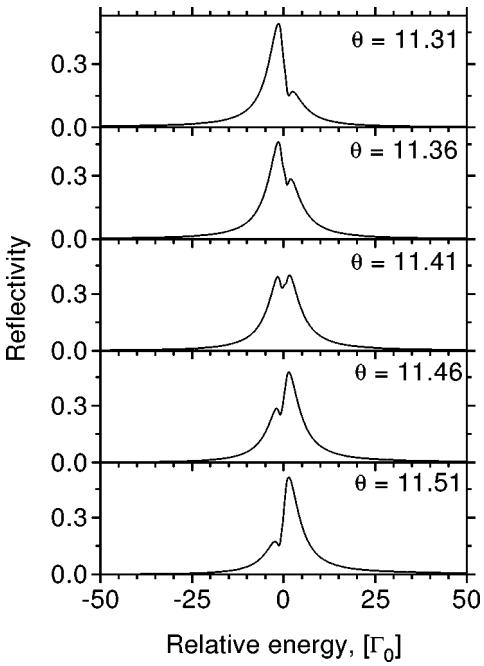

Figure 3. Computer simulation of the energy spectra of the first-order nuclear Bragg reflection for a [^{57}Fe(10)/^{56}Fe(30)] · 25 multilayer at different grazing angles in the vicinity of the precise Bragg angle of $\theta_B = 11.41$ mrad.

by a [^{57}Fe(10)/^{56}Fe(30)] · 25 multilayer for several grazing angles in the vicinity of the Bragg angle $\theta_B = 11.41$ mrad. At lower grazing angles the maximum reflectivity is shifted to lower energies and vice versa. The reason is that the complex increment $\tilde{\delta}$ of the refractive index contains an energy-dispersive nuclear contribution $\tilde{g}$ in the vicinity of the resonant energy E_0:

$$\tilde{\delta} = 2(\tilde{\chi} + \tilde{g}), \quad \tilde{g} = -\frac{\lambda\sigma_0 n f_{LM}\eta}{\nu + i}. \tag{2.3}$$

Here $\nu = 2(E - E_0)/\Gamma_0$ is the dimensionless deviation from the resonance energy, $\sigma_0 = 2.56 \times 10^{-18}$ cm^2 is the resonant cross-section for the 14.413 keV nuclear transition of the ^{57}Fe isotope, f_{LM} is the Lamb–Mössbauer factor, and η is the abundance of the resonant isotope. Equation (2.3) gives more negative refraction increment for $E > E_0$ and less negative (or even positive) for $E < E_0$. Therefore the critical angle is higher above and lower below the resonance. According to eq. (2.1), this shifts the Bragg angle to higher or lower values, respectively. Thus the energy spectrum of nuclear resonant diffraction is dominated by the low energy radiation at smaller angles and vice versa. A similar analysis for single crystals can be performed using the dynamical theory of nuclear resonant scattering [25,26]. In the case of multilayers the effect appears more pronounced, because it is stressed by the dip in the center of the energy spectrum (see below). The energy-dispersive refraction influences the

energy spectrum even stronger if the nuclear transition is split into several hyperfine components, because for each resonant line the alteration of the refractive index is enforced by the tails of the neighboring lines [10,11].

2.3. Double-peak energy spectrum

When the grazing angle matches the Bragg angle exactly, the energy spectrum of nuclear diffraction has a double-peak shape with a dip in the center (figures 3, 4). This shape of the energy spectrum has not been observed for single crystals, but is typical for periodic multilayers [3–5,11,29]. It occurs as a consequence of the small total thickness of the periodic multilayer and the large relative thickness of the resonant layer. As mentioned above, the Fresnel–Parratt formalism [7] and the dynamical theory of nuclear resonant diffraction [30] give an equivalent description of X-ray scattering by multilayers. Although we use the first approach for quantitative calculations, the double-peak energy spectra can be more easily explained in terms of the dynamical theory of nuclear resonant diffraction. The peculiar shape of the energy spectra results from the interference of two wave fields under the conditions of Bragg diffraction in the relatively thin periodic multilayer. Dynamical Bragg diffraction in an infinitely thick periodic multilayer is described by a single wave, whereas for the thin structure a second wave has to be taken into account as well. The amplitude and the phase of the second wave relative to the first one depend on the energy shift from the resonance.

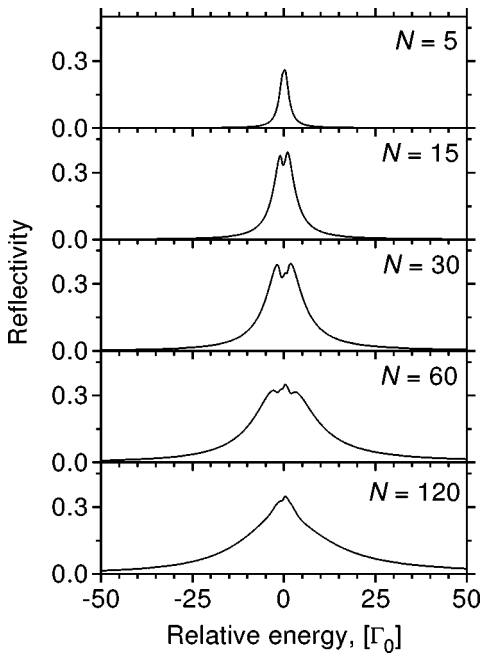

Figure 4. Computer simulation of the energy spectra of the first-order nuclear Bragg reflection for a $[^{57}\mathrm{Fe}(10)/^{56}\mathrm{Fe}(30)] \cdot N$ multilayer with different number of periods N.

For the sake of simplicity, we neglect the electronic refraction and absorption. Then the amplitudes R_1 and R_2 of the two reflected waves at the exact Bragg position can be obtained as

$$R_1 = \frac{-F}{1+h-(1-h)\exp(\mathrm{i}k\tilde{g}th\beta)}, \qquad R_2 = \frac{F\exp(\mathrm{i}k\tilde{g}th\beta)}{1+h-(1-h)\exp(\mathrm{i}k\tilde{g}th\beta)}, \quad (2.4)$$

where $\beta = d_{57}/d_0$ is the relative thickness of the resonant layer, $k = \lambda^{-1}$ is the wave vector of the incident radiation, $t = D/\sin\theta_\mathrm{B}$ is the total thickness of the multilayer along the X-ray beam, $h = \sqrt{1-F_m^2}$, and the structure factor F_m for the mth order reflection can be derived as

$$F_m = \frac{\sin(m\pi\beta)}{\pi\beta}. \quad (2.5)$$

If the energy of incident radiation is far away from the resonant energy, the exponent $\exp(\mathrm{i}k\tilde{g}th\beta)$ is close to unity. Therefore, the two waves have the same amplitudes but opposite phases. Their destructive interference cancels the diffraction intensity out of resonance. Approaching the resonance, both the ratio of the amplitudes $R = |R_2/R_1|$ and the phase difference Φ change with energy, nevertheless the amplitudes do so slower than the phase difference:

$$R(E) \cong \exp\left(-\frac{\xi}{\nu^2}\right) \cong 1 - \frac{\xi}{\nu^2}, \quad (2.6)$$

$$\Phi(E) \cong \pi - \frac{\xi}{\nu}, \quad (2.7)$$

where $\xi = h\beta T$, and $T = \sigma_0 n t f_{\mathrm{LM}}\eta$ is the effective resonant thickness of the multilayer along the X-ray beam. The two waves get exactly in phase when $\nu = \xi/\pi$. At this energy the diffraction intensity reaches its maximum. Closer to the resonance the waves get in anti-phase again, and the diffraction intensity drops. However, it no longer reaches zero, because the amplitude of the second wave R_2 is already essentially smaller than R_1. In the vicinity of the resonance the phase oscillates very fast, but the interference loses contrast, since the amplitude of the second wave vanishes. This produces the double-peak shape of the energy spectra. Accounting for the electronic absorption introduces some corrections into the above analysis. For instance, both amplitudes R_1 and R_2 approach zero out of resonance, and the second wave becomes less pronounced for thicker multilayers. A similar interference effect was observed in Laue diffraction of nuclear radiation in single crystals [31].

The double-peak shape of the energy spectrum is sensitive to the thickness of the multilayer. According to eqs. (2.6) and (2.7), for a very thin sample the waves get the same phases only very close to resonance, where the amplitude of the second wave R_2 is already negligible. Therefore the central dip in the energy spectrum does not appear (figure 4). For an intermediate thickness the waves get in phase at a distance of several natural linewidths from resonance, where the amplitudes R_1 and R_2 are comparable, and their effective interference produces the double-peak shape of the

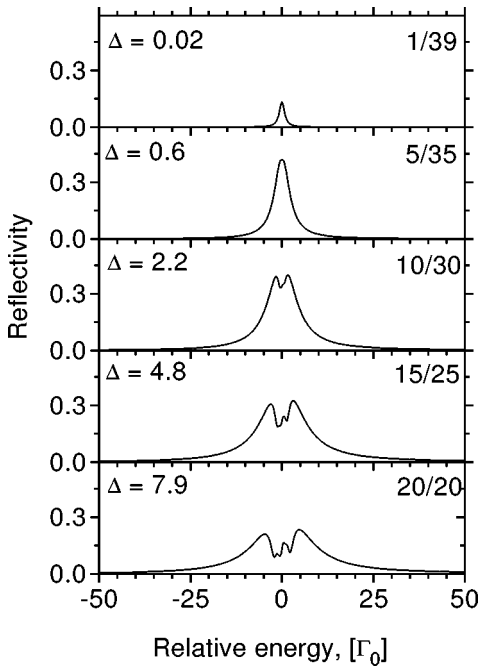

Figure 5. Computer simulation of the energy spectra of the first-order nuclear Bragg reflection for a $[^{57}\mathrm{Fe}(d_{57})/^{56}\mathrm{Fe}(d_{56})] \cdot 25$ multilayer with different relative thicknesses d_{57}/d_{56} of the resonant layer (indicated in the right-top corner). Note the good agreement between the splitting Δ estimated from eq. (2.8) and the calculations.

energy spectrum. For thicker samples the electronic absorption cancels the second wave, and the interference effect disappears again.

The double-peak shape of the energy spectrum appears only for periodic multilayers with a large relative thickness of the resonant layer, where the effect of suppression of inelastic channels of nuclear resonant scattering [19–22,25–28] is not fulfilled. This can be seen directly from eq. (2.7). The energy distance Δ between the two peaks of the energy spectrum can be estimated as

$$\Delta = \frac{\Gamma_0 h \beta T}{\pi}. \tag{2.8}$$

The splitting Δ depends on the relative thickness of the resonant layer $\beta = d_{57}/d_0$ explicitly and implicitly through the coefficient h. The higher the relative thickness of the resonant layer, the larger should be the energy splitting between the two peaks. This trend is demonstrated in figure 5. Note the good agreement between the splitting estimated through eq. (2.8) and the precise calculations.

The double-peak shape of the energy spectrum leads to dynamical beats in the time evolution of nuclear diffraction (figure 6). When the relative thickness of the resonant layer is small, the nuclear diffraction decreases monotonically with time. For thicker resonant layers beats appear and become more pronounced when the resonant

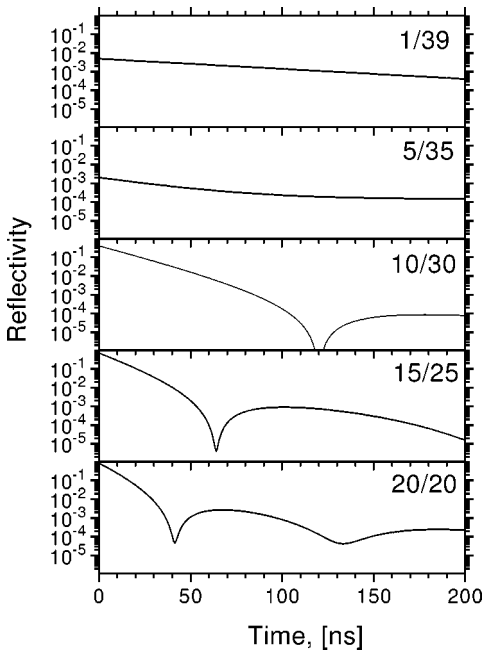

Figure 6. Computer simulation of the time dependence of the first-order nuclear Bragg reflection for a $[^{57}\mathrm{Fe}(d_{57})/^{56}\mathrm{Fe}(d_{56})] \cdot 25$ multilayer with different relative thicknesses d_{57}/d_{56} of the resonant layer (indicated in the right-top corner).

thickness is further increased. We note that these beats resemble the dynamical beats of nuclear forward scattering [32]. However, the modulation of the beat pattern in figure 6 is smaller. For instance, the minima do not reach the zero level.

2.4. Enhancement of the radiative channel of nuclear scattering

Since the angular width of the reflections for periodic multilayers is much larger than the angular divergence of the synchrotron radiation beam, the Bragg conditions can be fulfilled precisely in the experiment. This ensures an ideal coherence of the waves scattered by each reflecting plane and, therefore, provides optimal conditions for the enhancement of the radiative channel of nuclear scattering [19–22,25–28]. This effect shows up as a broad energy width of the diffraction spectrum (figures 4, 5) and a speed-up of the time evolution of nuclear diffraction (figure 6). The typical width of the energy spectrum is about $10–20\Gamma_0$ for a single-line nuclear transition (figures 4, 5) and may reach up to $30–40\Gamma_0$ if the transition consists of several unresolved hyperfine components [12]. In accordance with the large energy width, the time spectra of nuclear diffraction show a very fast decay. For instance, a decay time as small as 4 ns (figure 7) was observed in the time dependence of nuclear resonant diffraction of synchrotron radiation by a $[^{57}\mathrm{Fe}(22)/\mathrm{Sc}(11)/\mathrm{Fe}(22)/\mathrm{Sc}(11)] \cdot 25$ multilayer [13]. This has to be compared with the 141 ns natural lifetime of the nuclear transition.

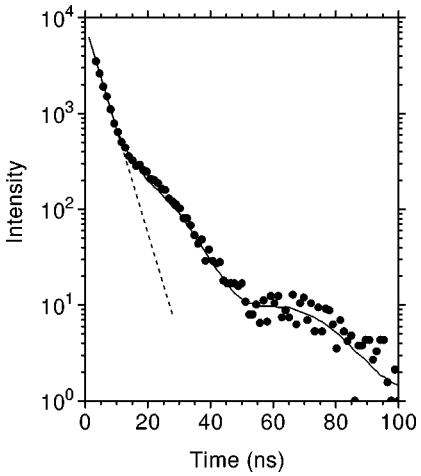

Figure 7. Time evolution of nuclear resonant Bragg scattering of synchrotron radiation by a [^{57}Fe(22)/Sc(11)/Fe(22)/Sc(11)] · 25 multilayer. The solid line is the dynamical diffraction theory fit. The dashed line indicates the initial decay with a lifetime of 4 ns. From [13].

3. Suppression of electronic scattering

Since the main motivation to apply periodic multilayers in nuclear resonant scattering was filtering the resonant components from the broad band energy spectrum of synchrotron radiation, much attention has been focused on the suppression of electronic scattering. Several options were proposed, and some of them were successfully employed in practice. In this section we present a short review of the approaches to obtain pure nuclear diffraction with periodic multilayers.

3.1. Isotope alteration

As discussed above, the most straightforward approach to obtain pure nuclear reflection with periodic multilayers is to alternate layers made of resonant and nonresonant isotopes of the same element [1]. The model ^{57}Fe/^{56}Fe periodic multilayer was examined with computer simulation [2–6] and promising perspectives were demonstrated. However, early attempts to produce such multilayers failed. One of the problems seems to originate from inter-layer diffusion. The diffusion of iron atoms is rather small for amorphous and single-crystalline material, but may increase along the grain boundaries. This may spoil the isotope alteration, therefore, the formation of a polycrystalline state with numerous grain boundaries has to be avoided during preparation. Another important point is the proper control of the homogeneity of individual layers during preparation.

It is difficult to avoid inter-layer diffusion in a sputtering process because when the thickness of the layer exceeds $\sim$30 Å, the spontaneous crystallization usually starts. In a first attempt to solve the problem, more complicated periodic multilayers were tried. In [11], the iron atoms were embedded into the matrix of the alloy

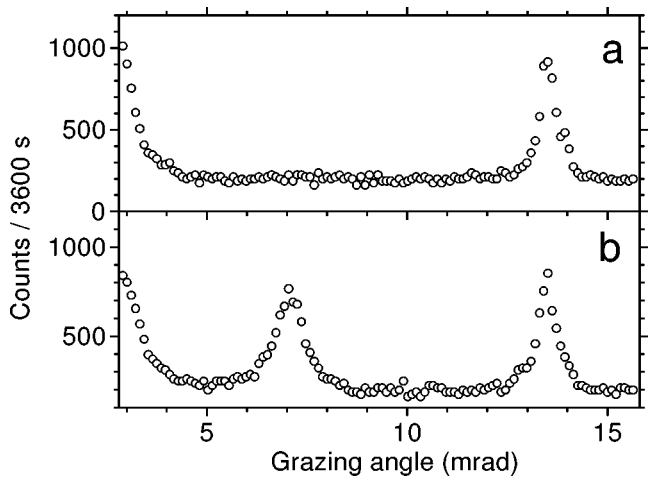

Figure 8. Angular dependence of scattering of nuclear γ-radiation from the radioactive Mössbauer source by a $[^{57}\mathrm{Fe}(22)/\mathrm{Sc}(11)/\mathrm{Fe}(22)/\mathrm{Sc}(11)]\cdot 25$ multilayer when the radiation was (a) out of resonance and (b) in resonance. From [12].

Fe_5B_4C, where the diffusion seems to be less and a $[^{56}Fe_5B_4C(48)/^{57}Fe_5B_4C(39)]\cdot 10$ periodic multilayer was prepared. In [12], inter-layer diffusion of iron atoms in a $[^{57}\mathrm{Fe}(22)/\mathrm{Sc}(11)/\mathrm{Fe}(22)/\mathrm{Sc}(11)]\cdot 25$ multilayer was suppressed using isolating Sc layers. Both multilayers exploited the idea of isotope alteration, deviating from the original $^{57}\mathrm{Fe}/^{56}\mathrm{Fe}$ concept only in technical details. They were investigated with the nuclear γ-radiation of Mössbauer sources, where the existence of pure nuclear reflections was demonstrated [11,12].

Figure 8 shows the angular dependence of scattering of nuclear γ-radiation from the Mössbauer source $^{57}\mathrm{Co}$ by a $[^{57}\mathrm{Fe}(22)/\mathrm{Sc}(11)/\mathrm{Fe}(22)/\mathrm{Sc}(11)]\cdot 25$ multilayer [12]. Two curves were recorded when the radiation was either off resonance (a) or in resonance (b) with the nuclear levels in the sample. The scattering out of resonance showed the tail of specular reflection at low angles and a first order reflection at a grazing angle of 13.5 mrad, which corresponds to the spatial period of 33 Å. In contrast, the curve measured at resonance has an additional peak at 7.0 mrad, which corresponds to the spatial period of 66 Å. This is pure nuclear reflection, which results from the isotope variation. The electronic reflectivity at the angular position of the pure nuclear reflection was as low as 1×10^{-3}. This periodic multilayer allowed the first successful application in a synchrotron radiation experiment [13]. The time spectrum of pure nuclear diffraction of synchrotron radiation was investigated, and the ability of the periodic multilayer to filter the resonant radiation for hyperfine nuclear spectroscopy was examined.

The problem of inter-layer diffusion was successfully overcome in later development of the preparation methods. Careful adjustment of growth parameters with the molecular beam epitaxy (MBE) technique allows one to prepare polycrystalline multilayers with a low fraction of grain boundaries. For instance, a good isotope separation

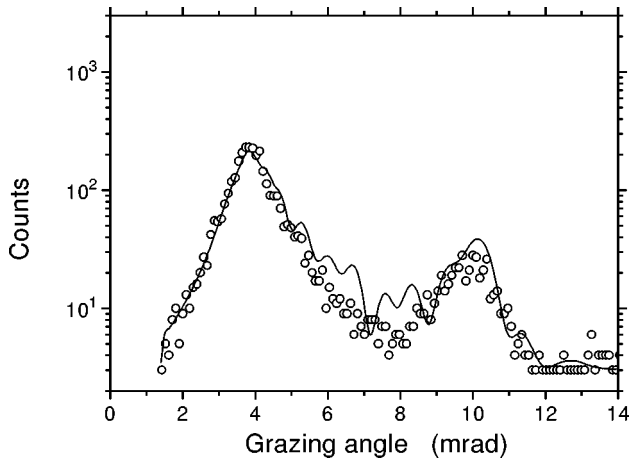

Figure 9. Angular dependence of nuclear scattering of synchrotron radiation by a [Fe(23.3)/^{57}Fe(23.3)] · 10 multilayer on a Zerodur substrate. The solid line shows the theory fit. From [33].

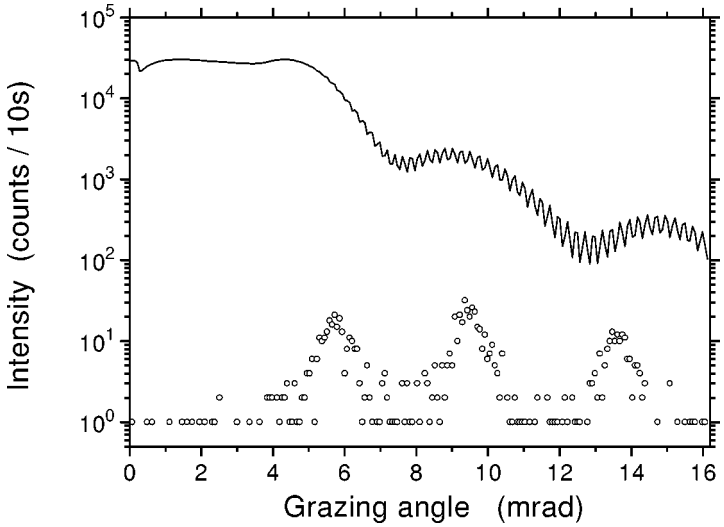

Figure 10. Angular dependence of nuclear (dots) and electronic (solid line) scattering of synchrotron radiation by a Pd(74)/[Fe(90)/^{57}Fe(10)] · 15 superlattice on a MgO(1 0 0) substrate. The electronic reflectivity is divided by 1000. From [35].

was achieved with a [Fe(23.3)/^{57}Fe(23.3)] · 10 multilayer on a Zerodur substrate [33]. Besides the total reflection peak, a significant pure nuclear Bragg reflection of the resonant synchrotron radiation was found (figure 9).

Almost complete suppression of inter-layer diffusion may be achieved with a single-crystalline periodic multilayer. This, for instance, was performed in [35] using ultra-high vacuum direct-current sputtering. Alternating layers of iron isotopes were sputtered on a single crystalline substrate of MgO(1 0 0). The isotope superlattice

Pd(74)/[Fe(90)/^{57}Fe(10)] · 15/MgO was prepared, which, in essence, is a single crystal of α-iron with spatial variation of the isotopic abundance. A top layer of Pd is included in order to prevent oxidation. The angular dependencies of electronic and nuclear scattering of synchrotron radiation by this superlattice are shown are figure 10. Electronic scattering exhibits Kiessig beats with two different periods. The fast beats correspond to the total thickness of the superlattice, the slow beats are caused by the top Pd layer. Nuclear scattering shows Bragg reflections of the first, second and third orders, which indicates the perfect isotope interfaces [35]. The first-order Bragg reflection overlaps another peak of nuclear scattering at the critical angle.

3.2. Antiferromagnetic multilayers

In order to obtain pure nuclear scattering of synchrotron radiation by a periodic multilayer one has to prepare different spatial periodicity of the amplitudes of nuclear and electronic scattering. In the approach of the isotope alteration this was achieved by varying the density of the resonant nuclei. Another means to alter the amplitude of nuclear resonant scattering is to exploit its sensitivity to the hyperfine magnetic and electric fields. The experience gathered in nuclear resonant scattering with single crystals reveals the existence of pure nuclear reflections for systems where the symmetry of the magnetic [36] or electric field [37] differs from that of the crystal lattice. For instance, in the case of a magnetic splitting, the amplitude of nuclear resonant scattering depends on the direction of the internal magnetic field at the nucleus. In particular, for a hyperfine transition with a change of the projection of the magnetic moment $\Delta J_z = \pm 1$, the polarization dependence of the complex amplitude of nuclear resonant scattering $\tilde{a}_\pm$ can be expressed [38] as

$$\tilde{a}_\pm \sim \big(\vec{h}_1 \cdot \vec{h}_2\big) - \big(\vec{h}_1 \cdot \vec{B}\big)\big(\vec{h}_2 \cdot \vec{B}\big) \mp \mathrm{i}\big(\big[\vec{h}_1 \times \vec{h}_2\big] \cdot \vec{B}\big), \tag{3.1}$$

where $\vec{h}_1$ and $\vec{h}_2$ are the unit vectors of the magnetic field in the incident and the scattered waves, respectively, and $\vec{B}$ is the real unit vector along the direction of the hyperfine magnetic field. Consider the scattering geometry where the hyperfine magnetic field $\vec{B}$ is directed either parallel or antiparallel to a $\vec{z}$ axis pointing along the direction of the incident beam. Neglecting the small angle of grazing incidence we obtain the scattering amplitudes $\tilde{a}^{\mathrm{R}}_\pm$ and $\tilde{a}^{\mathrm{L}}_\pm$ for radiation with right ($\vec{h}_{\mathrm{R}} = \vec{h}_x + \mathrm{i}\vec{h}_y$) and left ($\vec{h}_{\mathrm{L}} = \vec{h}_x - \mathrm{i}\vec{h}_y$) circular polarization, respectively, as

$$\tilde{a}^{\mathrm{R}}_\pm \sim 1 \mp \big(\vec{B} \cdot \vec{z}\big), \qquad \tilde{a}^{\mathrm{L}}_\pm \sim 1 \pm \big(\vec{B} \cdot \vec{z}\big). \tag{3.2}$$

This means, for instance, that the right circularly polarized radiation with an energy which corresponds to the hyperfine nuclear transition with $\Delta J_z = +1$ will be scattered only by those layers in which the hyperfine magnetic field is directed antiparallel to the direction of the incident radiation. For layers where the magnetic field is aligned parallel to the incident beam, the scattering amplitude equals zero. Therefore, an antiferromagnetic alignment of the hyperfine magnetic field in neighboring layers results

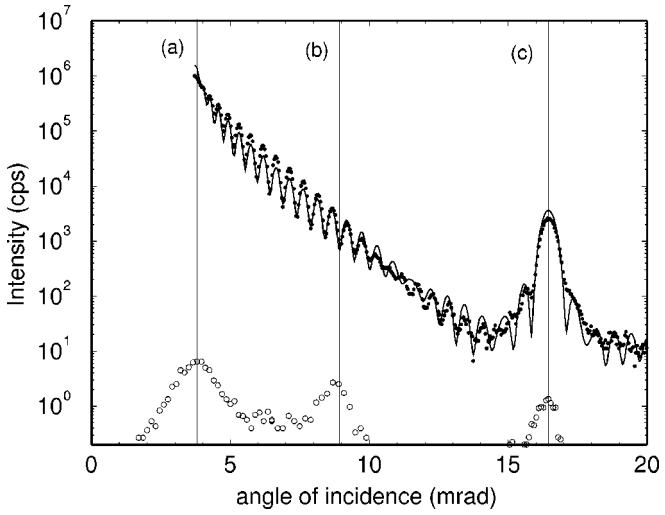

Figure 11. Angular dependence of the delayed nuclear (circles) and prompt electronic (dots) scattering of synchrotron radiation by a Cr(20)/[^{57}Fe(17)/Cr(10)] · 25/^{57}Fe(60) antiferromagnetic multilayer. The solid line shows the fit of the electronic reflectivity. The three vertical lines correspond to the angular positions of the (a) critical angle of the electronic total reflection, (b) antiferromagnetic pure nuclear Bragg reflection, and (c) first-order electronic Bragg reflection. From [14].

in a spatial variation of the amplitude of nuclear scattering, which leads to pure nuclear reflections. We note that the existence of pure nuclear reflection for an antiferromagnetic system is determined merely by the magnetic structure of the periodic multilayer and does not depend on the polarization properties of the incident radiation.

Multilayers with antiferromagnetic coupling of the neighboring layers are the subject of intense studies in solid state physics and in materials sciences, due to their unique magnetic properties such as giant magnetoresistance and the oscillation of the coupling constant with the thickness period [39]. Among them is the Fe/Cr system, which perfectly suits the purpose to achieve pure nuclear scattering of synchrotron radiation. Pure nuclear reflections for periodic Fe/Cr multilayers were observed with neutron reflectometry [40], which served as evidence for their antiferromagnetism. In the case of synchrotron radiation pure nuclear Bragg diffraction was achieved with a Cr(20)/[^{57}Fe(17)/Cr(10)] · 25/^{57}Fe(60) multilayer on a Zerodur substrate [14]. The angular dependence of electronic and nuclear scattering is shown in figure 11. The chemical periodicity of the multilayer with a period of 27 Å results in the first order electronic Bragg reflection at a grazing angle of 16.4 mrad. The same peak is seen also in the nuclear scattering. However, in contrast to electronic reflectivity, nuclear reflectivity shows a peak also at the angular position of the half-order reflections, which corresponds to a spatial period of 54 Å. This is the length of the periodicity of the magnetic superstructure which results from the antiferromagnetic coupling of the neighboring iron layers. The electronic reflectivity at this angular position is about 3×10^{-4}. In addition, there is a peak of the nuclear scattering at the position of the crit-

ical angle. Similar pure nuclear reflection was observed in a [FeSi(15.7)/ ^{57}Fe(25.5)]·10 antiferromagnetic multilayer [41].

3.3. Antireflecting coating

The residual electronic reflectivity at the angular position of pure nuclear reflection is determined by the specular reflection from the interfaces of the multilayer. As seen from the previous examples, this leads to the suppression of the electronic scattering by 3–4 orders of magnitude. Further reduction may be achieved with an additional antireflecting film [4]. This approach is identical to the GIAR-film (grazing incidence antireflection) technique [29,42,43]. The material and the thickness of the film is adjusted to provide destructive interference of the waves scattered from the air–film and film–multilayer boundaries. In comparison to the GIAR-films, the thickness of the antireflecting coating for a periodic multilayer should be larger because of the higher grazing angle. This makes the technique less sensitive to the imperfections of the fabrication processes and results in a larger angular width of the interference dip of the electronic reflectivity. In addition to the specular reflection from the top boundary, one may also consider suppressing the specular reflection from the bottom multilayer-substrate interface. According to computer simulations [4], the application of antireflecting films may reduce electronic scattering by the multilayer by several orders of magnitude.

3.4. Bragg antipeak

Isotope alteration and antiferromagnetic multilayers provide different spatial periodicity of the amplitudes of electronic and nuclear scattering. For this reason the peaks of electronic and nuclear diffraction are separated in angle. However, efficient suppression of the electronic scattering may also be achieved in the opposite case, when the amplitudes of electronic and nuclear scattering have identical spatial periods, so that each nuclear Bragg reflection is accompanied by an electronic one. Consider a multilayer which is composed of two elements with close electronic density nZ. This could be, for instance, a Tm/Fe periodic multilayer, where the relative variation of the electronic density is only 3.7%. Since the difference between the susceptibilities is small, an electronic reflection is essentially weak. With a proper choice of thickness of Tm and Fe layers the amplitude of the electronic Bragg reflection may match the amplitude of specular reflection from the top boundary. If the amplitudes of the two waves are in phase, the electronic scattering results in a peak at the Bragg position above the background of specular reflection. If, however, the waves are in anti-phase, the peak will be inverted, and the electronic Bragg reflection will appear as a sharp antipeak at the position of the Bragg angle [44]. This provides efficient suppression of electronic scattering even for the conditions of “nonpure” nuclear reflection. We note that the Bragg antipeak approach differs from the GIAR-film technique, since it uses the interference of the Bragg diffraction in order to suppress the specular reflection,

whereas in a GIAR-film the suppression is achieved by the interference of two specular reflected waves.

4. Characterization of multilayers and thin films with nuclear resonant scattering of synchrotron radiation

Grazing incidence nuclear resonant scattering of X-rays combines the advantages of hyperfine nuclear spectroscopy with the structure analysis potential of coherent scattering. In contrast to "incoherent" spectroscopic techniques (for instance, conversion electron Mössbauer spectroscopy), the physical process involved is collective coherent scattering by the ensemble of nuclei. The relative phases of the waves, scattered by various nuclei, do matter and essentially influence the experimental data. This

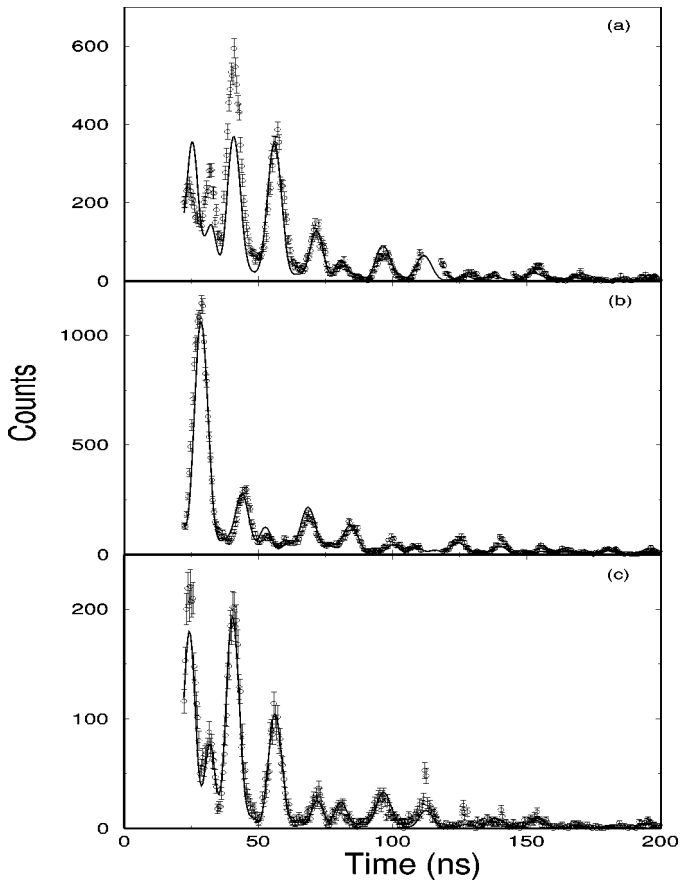

Figure 12. Time evolution of nuclear resonant scattering of synchrotron radiation by a Cr(20)/[^{57}Fe(17)/Cr(10)] · 25/ ^{57}Fe(60) antiferromagnetic multilayer at the three different angular positions (a)–(c) as indicated in figure 11. The fit of each time spectrum (solid lines) was achieved with the same parameters of the multilayer. From [14].

provides the sensitivity to the positions of the scattering centers and, therefore, gives the potential of site-selective hyperfine nuclear spectroscopy. Moreover, grazing incidence scattering is an easy means of controlling the thickness of the irradiated layer. This forms the basis for depth-selective hyperfine spectroscopy. In this section we review recent experimental work on the investigation of multilayers and thin films using nuclear resonant scattering of synchrotron radiation.

4.1. Site-selective hyperfine spectroscopy

An example of site-selective hyperfine nuclear spectroscopy is shown in figure 12. The time spectra of nuclear resonant grazing incidence scattering of X-rays by a Cr(20)/[^{57}Fe(17)/Cr(10)] · 25/ ^{57}Fe(60) periodic multilayer were measured at three different grazing angles: at the position of the critical angle (zero-order reflection), at the pure nuclear half-order reflection, and at the first order reflection [14]. The change of the angular position leads to changes in the relative phases of the waves which are scattered by the various layers. Therefore, the pattern of the quantum beats, which is essentially the image of the hyperfine structure, differs significantly for various grazing angles, even though the same layers contribute to each spectrum. This sensitivity was employed for the site-selective hyperfine analysis of the multilayer. The 17 Å layer of ^{57}Fe was divided into five sublayers, with their thickness and distribution of the magnetic hyperfine field chosen to be consistent with the results of conversion elec-

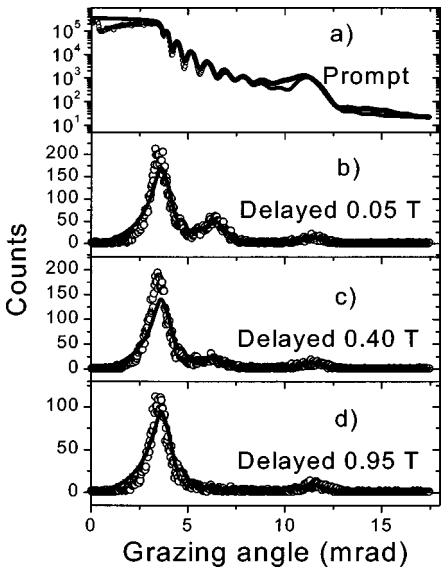

Figure 13. Angular dependence of prompt electronic and delayed nuclear scattering of synchrotron radiation by a [FeSi(25.5)/ ^{57}Fe(15.7)] · 10 multilayer on a Zerodur substrate in various external magnetic fields. The transition from the antiferromagnetic to the ferromagnetic state with increasing external field is seen as a vanishing of the pure nuclear reflection at 6.3 mrad. The fit curves correspond to the model described in [41]. From [47].

tron Mössbauer spectroscopy. The properties of these sublayers were supposed to be identical for all ^{57}Fe layers of the structure. The model assumed a correlation of the hyperfine magnetic field with the distance to the Fe/Cr interface. The fit shows that the resonant layer possesses six different hyperfine field distributions segregated into a 1–2–11–2–1 Å structure. The averaged hyperfine field of the sublayers decreases as one approaches the Fe/Cr interface. The central sublayer had a magnetic field of 33.3 T, the two neighboring sublayers had a field distribution centered at 30.7 T, whereas the two sublayers at the interface had a magnetic field distribution between 20 and 26 T. The fit of all three spectra was achieved with identical hyperfine and structural parameters, which puts rigid constraints on the model of the distribution of the hyperfine magnetic field over the thickness of the resonant layer.

Another example of site-selective hyperfine nuclear spectroscopy is shown in figures 13 and 14. The angular dependence of nuclear reflectivity of a [FeSi(25.5)/ ^{57}Fe(15.7)] $\cdot$ 10 multilayer on a zerodur substrate was measured for various external magnetic fields ($0 < B_{\text{ext}} < 0.95$ T) perpendicular to the scattering plane [45]. At room temperature the Fe/(FeSi) multilayers exhibit antiferromagnetic coupling of the neighboring iron layers [46]. Electronic reflectivity (figure 13) shows the first-order Bragg reflection at 11.7 mrad and damped Kiessig oscillations corresponding to the total film thickness of 412 Å. Nuclear scattering, in contrast, clearly reveals the periodicity of the magnetic structure with the doubled spatial period (antiferromagnetic Bragg reflections at 6.3 mrad), which gradually disappears with increasing transversal magnetic field. This shows that the magnetic moments of the antiferromagnetically coupled neighboring Fe layers gradually become canted by the increased magnetic field and the antiferromagnetic structure is fully suppressed at $B_{\text{ext}} = 0.95$ T. Thus, similar to X-ray grazing incidence scattering, the measurements of angular dependence of nuclear reflectivity provide a precise characterization of the spatial structure of nuclear resonant layers. As shown above, due to the sensitivity of nuclear scattering to the hyperfine magnetic field, this also enables an analysis of the magnetic structure of multilayers. Since the technique has much in common with neutron reflectometry, it is also called Synchrotron Mössbauer Reflectometry [16,33,41,45,47].

The time evolution of grazing incidence nuclear scattering reveals more subtle details of the magnetic structure and the coupling within the multilayer. In particular, the model of pure antiferromagnetic coupling of the neighboring Fe layers in a low ($B_{\text{ext}} = 0.05$ T) external magnetic field (dotted line) shows poor agreement with the data (figure 14). For instance, at low grazing angles it does not reproduce the distinct minimum at $\sim$28 ns after the excitation. Much better agreement was achieved with another model (solid line), which assumes strong antiferromagnetic coupling of the top eight layers, a ferromagnetic coupling between the two bottom layers and a weak coupling of the two regions [41]. This model is in agreement with the results of surface magneto-optic Kerr effect studies [48].

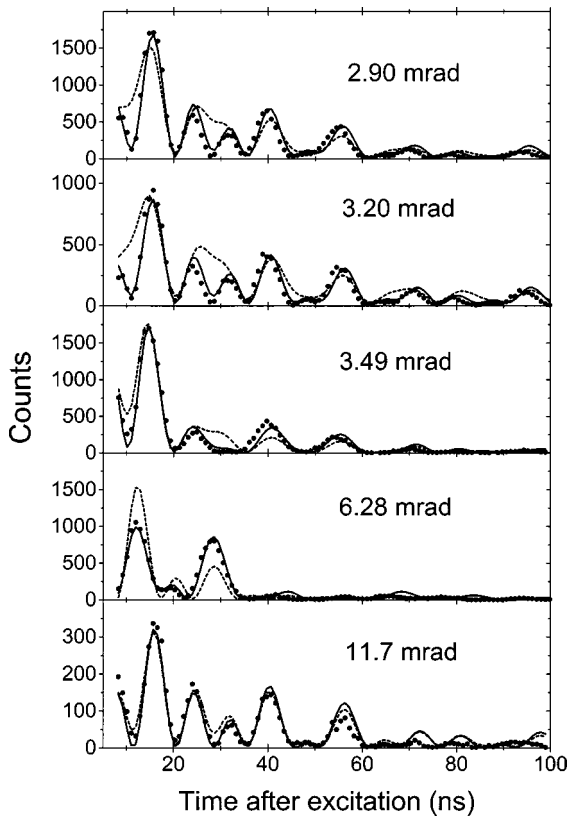

Figure 14. Time evolution of nuclear scattering of synchrotron radiation by a [FeSi(25.2)/^{57}Fe(15.7)]·10 multilayer on a Zerodur substrate in an external field of 0.05 T perpendicular to the scattering plane at different grazing angles. The dotted line is the fit corresponding to the antiferromagnetic model. The solid line shows the fit which assumes the antiferromagnetic coupling of the eight top layers and the ferromagnetic coupling of the two bottom layers [41]. From [47].

4.2. Depth-selective hyperfine spectroscopy

Site-selectivity of hyperfine nuclear spectroscopy in the examples above was achieved mainly by measuring the time spectra of nuclear scattering at the angular positions of different order reflections, which varies the phase relations between the waves scattered by different sublayers. This approach allows one to choose the nuclear sites in an arbitrary way, according to the experimental task. For instance, the choice may correlate with the proximity of nuclei to the interface between the layers [14]; or with the location of nuclei relative to the multilayer surface [45]. The latter type of *depth*-selective analysis may also be performed by measuring the time spectra of nuclear scattering in the vicinity of the critical angle. The penetration depth of X-rays in this angular region strongly depends on the grazing angle and decreases to a few nanometers below the critical angle. Therefore, measurements of the time spectra of nuclear scattering as a function of increasing grazing angle enables sampling the hy-

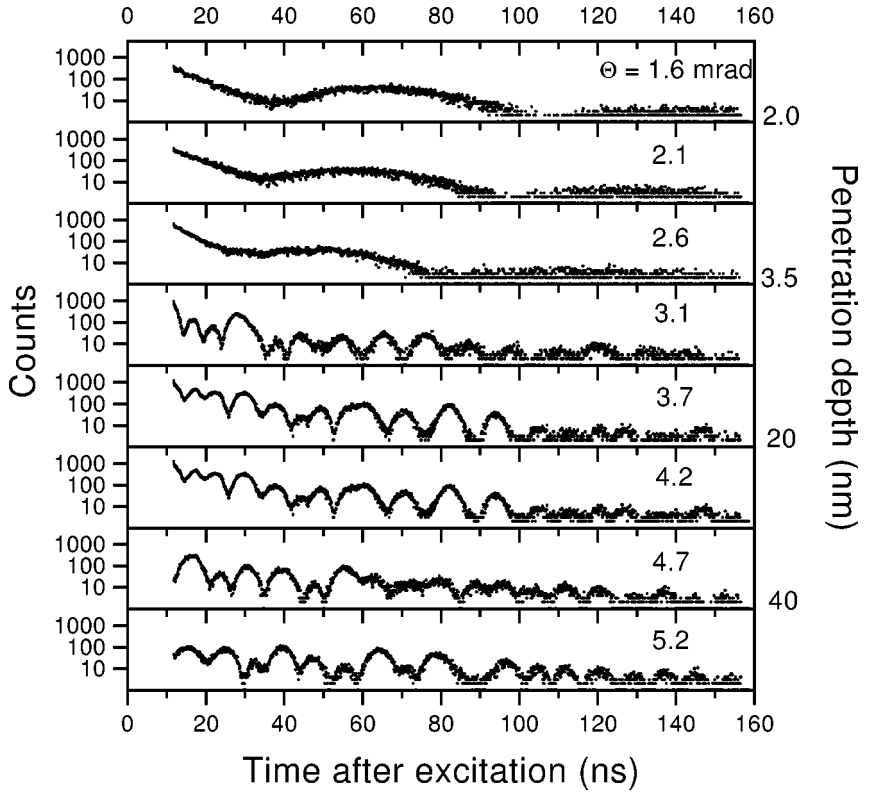

Figure 15. Time evolution of grazing incidence nuclear resonant scattering of synchrotron radiation by an originally 20 nm thick ^{57}Fe film grown onto a float glass substrate and exposed to annealing in air at 170°C for 4 h. The grazing angle is indicated in the right-top corners. The penetration depth of photons is shown on the right-hand vertical axis. From [47].

perfine nuclear structure in surface layers of increasing thickness. Such measurements allow one to obtain the depth profiles of hyperfine nuclear parameters. This approach is especially important for nonperiodic multilayers and thin films, where the peak of nuclear reflectivity at the critical angle is the main chance to reach a significant count rate.

An example of the depth-selective hyperfine spectroscopy of thin films is shown in figure 15. The time spectra of nuclear resonant scattering of synchrotron radiation by an originally 200 Å, thick α-^{57}Fe film oxidized for 4 h at 170°C in air was measured at various grazing angles [45,47]. The penetration depth (indicated on the right-hand vertical axis) for the three lowest spectra is comparable to the total thickness of the film. Therefore these spectra correspond to the bulk of the film. The fast beats are characteristic for α-Fe and a spontaneously magnetized iron oxide, probably Fe_3O_4. For the upper three spectra the penetration depth was about 20–30 Å, corresponding to about ten top atomic layers. No magnetic interaction is seen in these spectra. The upper layer could probably be assigned to paramagnetic β-FeOOH and to superparamagnetic α-Fe_2O_3. The clear difference of the time spectra of nuclear scattering for

the same sample at different grazing angles demonstrates the high depth selectivity of this technique. It is worth mentioning that the characterization of the sample took only about 20 min of measuring time for each time spectrum.

4.3. Site-selective hyperfine spectroscopy using selective deposition

By varying the grazing angle of the specular reflection one can obtain a depth resolution of about several nanometers. Further improvement of the depth selectivity requires controlled deposition techniques like MBE, where the resonant isotope is deposited selectively on to the distinct layer one wants to investigate. This allows, for instance, the precise analysis of the magnetic structure of thin layers as a function of their proximity to the interface. The sensitivity of nuclear scattering is sufficient for hyperfine spectroscopy on a single monolayer [15]. Similar sensitivity may be achieved with depth-selective conversion electron spectroscopy. However, in the latter case the signal-to-noise ratio is 1% or less, whereas the nuclear scattering is essentially free from the background. In addition, nuclear scattering is more favorable for experiments in high magnetic fields and at variable temperature, which are difficult for electron spectrometers.

4.3.1. Single magnetic monolayer

The limit of sensitivity in grazing incidence nuclear scattering was examined with Fe/Au bilayers [15]. The samples were grown by MBE on Ge(0 0 1) substrates. For preliminary studies three samples were prepared. Two of them (A and B) consisted of 40 monolayers (1 monolayer = 1.43 Å) of natural Fe, followed by 10 monolayers of ^{57}Fe, then by 5 monolayers of natural Fe, and finally covered by $\sim$20 Å of Au in order to prevent oxidation. We denote these samples as Au/5Fe/10^{57}Fe/40Fe/Ge. The composition of the third sample (C) was Au/2Fe/4^{57}Fe/5Fe/Ge. The first sample was grown at 200°C, the others at room temperature, using an ultrathin layer of sulphur as a surfactant, promoting layer-by-layer growth.

The time spectra of nuclear resonance grazing incidence scattering measured at room temperature at a grazing angle of 4–5 mrad are shown in figure 16. The solid lines are theoretical fits. A polarizing field of 15–44 mT was applied in the horizontal plane, perpendicular to the beam direction. The time spectra for samples A and B have pronounced quantum beats, which result from scattering via the simultaneous excitation of four hyperfine transitions with $\Delta J_z = \pm 1$. The best fits were obtained with the linewidth of the nuclear transition $\Gamma = 1.30(5)\Gamma_0$. This suggests a probe layer with a good structural quality. A significant improvement of the fit was achieved by allowing for a second, nonmagnetic, phase with a random orientation of the electric field gradient. The relative intensity of the nonmagnetic phase was 6(1)% for both samples.

In contrast to the other samples, the spectrum for sample C shows no “magnetic” quantum beats. It could be fit reasonably well with a combination of two nonmagnetic components of roughly equal intensities. The average quadrupole splitting is very close

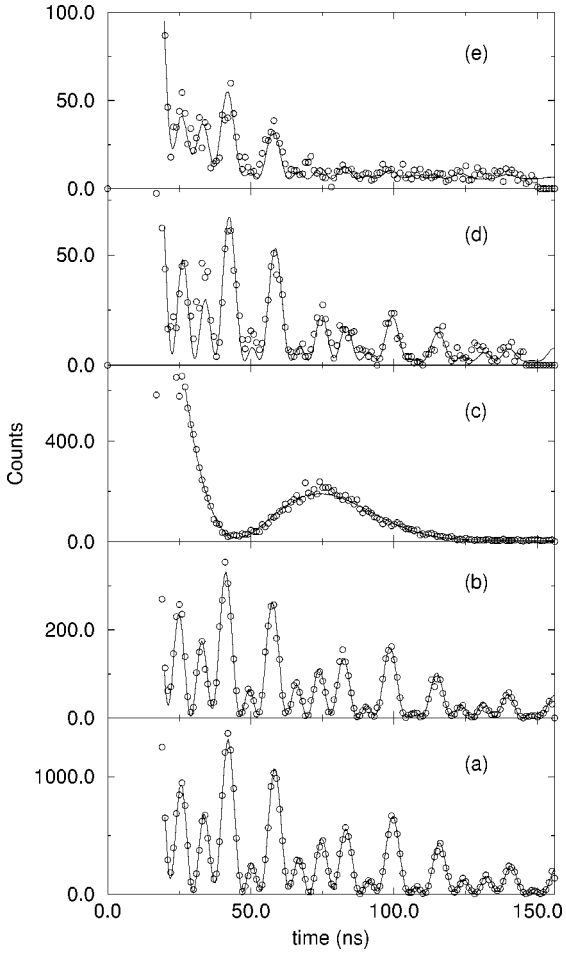

Figure 16. Time spectra of nuclear resonant grazing incidence scattering of X-rays by five different Au/Fe multilayers on a Ge substrate: (a) sample A, grazing angle $\theta = 4.7$ mrad, (b) sample B, $\theta = 4.7$ mrad, (c) sample C, $\theta = 4.7$ mrad, (d) sample D, $\theta = 4.0$ mrad, and (e) sample E, $\theta = 5.2$ mrad. The solid lines show the theory fit. From [15].

to that found for the nonmagnetic components of samples A and B, suggesting a common origin. The similarity of the hyperfine parameters of the nonmagnetic components to those of the crystalline and amorphous Ge/Fe phases allowed authors to associate this component with interdiffusion of Fe and Ge.

In an attempt to avoid this interdiffusion the final two samples with a single monolayer of the resonant isotope were grown without the sulphur surfactant. Compositions of the samples (D and E) were Au/4Fe/1^{57}Fe/10Fe/Ge and Au/1^{57}Fe/14Fe/Ge, respectively. The corresponding time spectra are shown in figures 16(d), (e). The fit gives no indication of the formation of a Fe/Ge interlayer. On the other hand, the large linewidth for samples D and E, 3.4(5)Γ_0 and 5.5(1.5)Γ_0, respectively, is associated

with a distribution of the hyperfine magnetic fields. This points to a lower structural quality of the resonant isotope layer than in the case of samples A–C, which is in agreement with other reports on the growth of Fe on Ge(1 0 0) [49]. The relatively broad distribution of the magnetic field causes the damping of the nuclear scattering at later times. The data clearly show that a sensitivity to a single monolayer of ^{57}Fe is achieved.

4.3.2. Superparamagnetic multilayers

Thin films of magnetite Fe_3O_4 attract much interest due to the combination of high magnetic ordering temperature ($T_C = 858$ K), completely spin-polarized electronic transport, and superparamagnetic behavior. Magnetite has the cubic spinel structure. The Fe^{3+} ions at the tetrahedral A-sites couple antiferromagnetically with the iron ions at the octahedral B-sites. The charge on the B-site ions is 2.5+ on average. At room temperature the extra electrons hop between the B-sites at a rate which is much faster than the nuclear precession frequency. The Mössbauer spectrum consists of two magnetic sextets, which correspond to the A- and B-sites. Fe^{2+}/Fe^{3+} charge ordering at the B-sites occurs below the Verwey transition at 120 K. This transition is associated with subtle structural changes that are still not completely understood. The resulting Mössbauer spectrum is also complicated: whereas the A-site contribution is a single sextet, the B-site contribution has been fitted with a varying number of components up to five [50].

A suitable substrate for the epitaxial growth of Fe_3O_4 films is MgO(1 0 0), because the lattice constants of the oxygen sublattices match within 0.3%. Nevertheless, thin magnetite films on this substrate show a thickness dependent decrease of the saturation magnetization. The effect has been explained with nonmagnetic or disordered "dead" interface layers of 7 Å thickness [51]. However, this interpretation was not confirmed by recent Mössbauer data, where superparamagnetic behavior was observed through the entire thickness of the film [52].

In order to clarify the problem, the same samples as used in [52] were studied with nuclear resonant grazing incidence scattering at various temperatures between 15 and 150 K [53]. The composition of the samples was $[8MgO/8Fe_3O_4] \cdot 5/MgO(1\,0\,0)$. For these systems one monolayer denotes the 2.1 Å distance between two successive oxygen layers (the lattice constant of magnetite is 8.39 Å, i.e., four monolayers). Two probe monolayers of ^{57}Fe nuclei were inserted either at the center, or at the interface of the magnetite layers. The measurements were performed at 15 K, with an external magnetic field of 0.23 T applied in the horizontal plane, perpendicular to the X-ray beam. Figure 17 shows the time spectra of nuclear scattering for two samples with the "bulk" and the "interface" probe layers. The spectra are practically identical, confirming the absence of the "dead" layer. The spectra are fit with a coherent sum of three components, one for the A-site Fe^{3+} ions and two for the B-site Fe^{2+}/Fe^{3+} ions.

Figure 18 shows the time spectra of nuclear scattering for the "bulk" sample at three different temperatures. The data taken at 15 K do not show any trace of

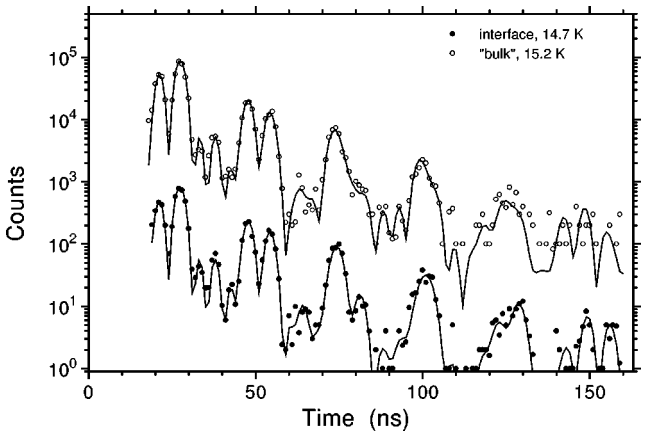

Figure 17. Time spectra of nuclear grazing incidence scattering of X-rays by two $[8MgO/8Fe_3O_4] \cdot 5$ multilayers on a MgO(1 0 0) substrate at low temperature. The "bulk" sample contained two probe monolayers of ^{57}Fe nuclei in the center of the Fe_3O_4 layers. The "interface" sample had two probe monolayers of ^{57}Fe nuclei at the Fe_3O_4/MgO interface. The grazing angle was 2.8 mrad. Solid lines show the theory fit. To facilitate comparison, the "bulk" spectrum has been shifted vertically by multiplying by 100. From [53].

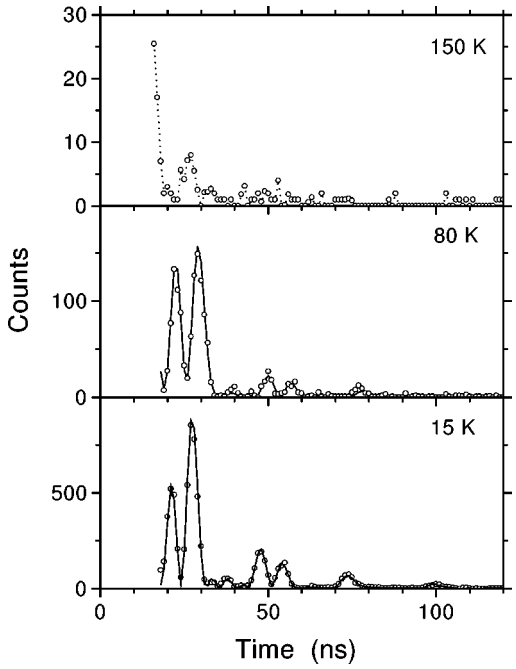

Figure 18. Time spectra of nuclear grazing incidence scattering of X-rays by a $[8MgO/8Fe_3O_4] \cdot 5$ multilayer on a MgO(1 0 0) substrate, with two probe monolayers of ^{57}Fe in the center of the Fe_3O_4 layers, for three different temperatures. The grazing angle was 2.8 mrad. The dashed line is to guide the eye, solid lines show the theory fit. From [53].

fluctuating magnetic fields. In contrast, at 80 K the damping at later times increased considerably and the average hyperfine field is 9% lower than at 15 K. This behavior is associated with magnetization fluctuations in the entire ferrimagnetic domain [54]. The data at 150 K show a nearly structureless spectrum with very fast damping, as expected for the situation in which the nuclear precession time ($\sim$15 ns) is roughly equal to the characteristic time between magnetization reversals.

5. Summary

Periodic multilayers were introduced to nuclear resonant scattering in order to obtain super-narrow monochromatization of synchrotron radiation. The aim was reached: pure nuclear reflection of synchrotron radiation was achieved with several multilayers [13,14,33,35,41]. The feasibility of hyperfine spectroscopy using periodic multilayers as a monochromator with super-narrow energy resolution was examined [13]. In comparison to resonant monochromators which are based on grazing incidence anti-reflection films [42,43], periodic multilayers provide a somewhat narrower energy bandwidth. For instance, an energy width of about $40\Gamma_0$ was achieved in [13]. Since this is smaller than the typical splitting of nuclear levels, hyperfine spectroscopy with this type of monochromator is not straightforward. With the GIAR-films one may reach about $150\Gamma_0$ [42,43], which is more preferable for hyperfine spectroscopy. However, the periodic multilayers showed a better suppression of the electronic scattering. An electronic reflectivity as low as 10^{-3} may be easily achieved [13,14] with the periodic multilayers, whereas the GIAR-films may offer about 10^{-2} [55]. At the present state of research the filtering application of the periodic multilayers is pending, since the competitive development of high-resolution monochromators [56] and fast detectors [57] mostly solved the problem of high radiation flux at the third generation sources of synchrotron radiation. However, this may change with the advent of the next generation sources.

The exploration of the field of nuclear resonant grazing incidence scattering by multilayer structures shows high potential for the characterization of the multilayer samples. The combination of hyperfine spectroscopy with site-selective structure analysis creates a powerful technique. It benefits significantly from the outstanding properties of synchrotron radiation, such as high spectral density, narrow angular collimation, small beam size and linear polarization.

Acknowledgements

A.C. is grateful to U. van Bürck, R. Röhlsberger, and G.V. Smirnov for helpful discussions and to B. Hjörvarsson for the permission to use his unpublished results. D.L.N. is grateful to A.Q.R. Baron, L. Bottyán, L. Deák, O. Leupold, R. Rüffer and H. Spiering for helpful discussions, as well as to the Hungarian Scientific Research Fund (OTKA) for financial support (contract no. T016667).

References

[1] G.T. Trammel, J.P. Hannon, S.L. Ruby, P. Flinn, R.L. Mössbauer and F. Parak, AIP Conf. Proc. 38 (1977) 46.
[2] V.A. Kabanic, Version of a nuclear resonance filter for Mössbauer diffraction with synchrotron radiation, preprint, Institute of Nuclear Physics, Novosibirsk (1989).
[3] A.I. Chumakov and G.V. Smirnov, JETP Lett. 53 (1991) 271 (Pis'ma Zh. Eksper. Teoret. Fiz. 53 (1991) 258).
[4] M.V. Gusev, A.I. Chumakov and G.V. Smirnov, JETP Lett. 58 (1993) 257 (Pis'ma Zh. Eksper. Teoret. Fiz. 58 (1993) 251).
[5] L. Deák, L. Bottyán and D.L. Nagy, in: *Condensed Matter Studies by Nuclear Methods, Proc. of the 28th Zakopane School of Physics*, Zakopane (1993), eds. E.A. Görlich and K. Tomala (Institute of Physics, Jagellonian University, and H. Niewodniczanski Institute of Nuclear Physics, Kraków, 1993) p. 269.
[6] L. Deák, L. Bottyán and D.L. Nagy, Hyp. Interact. 92 (1994) 1083.
[7] L.G. Parratt, Phys. Rev. 45 (1954) 359.
[8] J.P. Hannon, G.T. Trammel, M. Mueller, E. Gerdau, R. Rüffer and H. Winkler, Phys. Rev. B 32 (1985) 6374.
[9] R. Röhlsberger, this issue, section III-1.3.
[10] A.I. Chumakov, G.V. Smirnov, S.S. Andreev, N.N. Salashchenko and S.I. Shinkarev, JETP Lett. 54 (1991) 216 (Pis'ma Zh. Eksper. Teoret. Fiz. 54 (1991) 220).
[11] R. Röhlsberger, E. Witthoff, E. Lüken and E. Gerdau, J. Appl. Phys. 74 (1993) 1933.
[12] A.I. Chumakov, G.V. Smirnov, S.S. Andreev, N.N. Salashchenko and S.I. Shinkarev, JETP Lett. 55 (1992) 509 (Pis'ma Zh. Eksper. Teoret. Fiz. 55 (1992) 495).
[13] A.I. Chumakov, G.V. Smirnov, A.Q.R. Baron, J. Arthur, D.E. Brown, S.L. Ruby, G.S. Brown and N.N. Salashchenko, Phys. Rev. Lett. 71 (1993) 2489.
[14] T.S. Toellner, W. Sturhahn, R. Röhlsberger, E.E. Alp, C.H. Sowers and E.E. Fullerton, Phys. Rev. Lett. 74 (1995) 3475.
[15] L. Niesen, M.F. Rosu, A. Mugarza, R. Coehoorn, R.M. Jungblut, F. Rooseboom, A.Q.R. Baron, A.I. Chumakov and R. Rüffer, Phys. Rev. B 58 (1998) 8590.
[16] D.L. Nagy, L. Bottyán, L. Deák, E. Gerdau, V.N. Gittsovich, J. Korecki, O. Leupold, H. Reuther, V.G. Semenov and E. Szilágyi, in: *Condensed Matter Studies by Nuclear Methods, Proc. of the 32th Zakopane School of Physics*, Zakopane (1997), eds. E.A. Görlich and K. Latka (Institute of Physics, Jagellonian University, and H. Niewodniczanski Institute of Nuclear Physics, Kraków, 1997) p. 17.
[17] D. Rüter, R. Rüffer and E. Gerdau, this issue, section IV-1.1.
[18] A.M. Afanas'ev and O.G. Melikyan, Phys. Status Solidi A 122 (1990) 459.
[19] G.T. Trammel, in: *Proc. of Internat. Atomic Energy Agency Symp. on Chemical Effects of Nuclear Transformations*, Prague (1960), Vol. 1 (IAEA, Vienna, 1961) p. 75.
[20] A.M. Afanas'ev and Yu. Kagan, JETP Lett. 2 (1965) 81 (Pis'ma Zh. Eksper. Teoret. Fiz. 2 (1965) 130).
[21] A.M. Afanas'ev and Yu. Kagan, JETP Lett. 21 (1965) 215 (Zh. Eksper. Teoret. Fiz. 48 (1965) 327).
[22] Yu. Kagan, A.M. Afanas'ev and V.G. Kohn, J. Phys. C: Solid State Phys. 12 (1979) 615.
[23] H. Kiessig, Ann. Phys. (Paris) 10 (1931) 769.
[24] A.Q.R. Baron, J. Arthur, S.L. Ruby, A.I. Chumakov, G.V. Smirnov and G.S. Brown, Phys. Rev. B 50 (1994) 10354.
[25] U. van Bürck, G.V. Smirnov, R.L. Mössbauer, H.J. Maurus and N. Semioschkina, J. Phys. C: Solid State Phys. 13 (1980) 4511.
[26] Y. Shvyd'ko and G.V. Smirnov, J. Phys. C: Condens. Matter 1 (1989) 10563.
[27] U. van Bürck, R.L. Mössbauer, E. Gerdau, R. Rüffer, R. Hollatz, G.V. Smirnov and J.P. Hannon, Phys. Rev. Lett. 59 (1987) 355.

[28] U. van Bürck, G.V. Smirnov, R.L. Mössbauer and T. Hertrich, J. Phys. C: Condens. Matter 2 (1990) 3989.
[29] R. Röhlsberger, Ph.D. thesis, Hamburg University (1994). Also in Internal Report, DESY, HASYLAB 94-06 (December 1994).
[30] A.M. Afanas'ev and Y. Kagan, JETP 37 (1973) 987 (Zh. Eksper. Teoret. Fiz. 64 (1973) 1958).
[31] G.V. Smirnov, V.V. Mostovoi, Y.V. Shvyd'ko, V.N. Seleznev and V.V. Rudenko, JETP Lett. 51 (1980) 603 (Zh. Eksper. Teoret. Fiz. 78 (1980) 1196).
[32] U. van Bürck, this issue, section IV-2.1.
[33] L. Deák, G. Bayreuther, L. Bottyán, E. Gerdau, J. Korecki, E.I. Kornilov, H.J. Lauter, O. Leupold, D.L. Nagy, A.V. Petrenko, V.V. Pasyuk-Lauter, H. Reuther, E. Richter, R. Röhlsberger and E. Szilágyi, J. Appl. Phys. 85 (1999) 1.
[34] R. Rüffer and A.I. Chumakov, Hyp. Interact. 97/98 (1996) 589.
[35] B. Hjörvarsson, unpublished (measured at ID18 at the ESRF [34]).
[36] G.V. Smirnov, V.V. Sklyarevsky, R.A. Voskanyan and A.N. Artem'ev, JETP Lett. 9 (1970) 70 (Pis'ma Zh. Eksper. Teoret. Fiz. 9 (1969) 123).
[37] R.M. Mirzababaev, G.V. Smirnov, V.V. Sklyarevsky, A.N. Artem'ev, A.N. Izrailenko and A.V. Babkov, Phys. Lett. A 37 (1971) 441.
[38] G.V. Smirnov, Prof. thesis, Kurchatov Institute of Atomic Energy, Moscow (1980).
[39] T. Shinjo, Surf. Sci. Rep. 21 (1991) 49.
[40] N. Hosoito, S. Araki, K. Mibu and T. Shinjo, J. Phys. Soc. Japan 59 (1990) 1925.
[41] L. Bottyán, J. Dekoster, L. Deák, A.Q.R. Baron, S. Degroote, R. Moons, D.L. Nagy and G. Langouche, Hyp. Interact. 113 (1998) 295.
[42] R. Röhlsberger, E. Gerdau, M. Harsdorff, O. Leupold, E. Lüken, J. Metge, R. Rüffer, H.D. Rüter, W. Sturhahn and E. Witthoff, Europhys. Lett. 18 (1992) 561.
[43] R. Röhlsberger, this issue, section IV-1.3.
[44] V.G. Kohn, A.I. Chumakov and R. Rüffer, JETP Lett. 87 (1998) 1 (Zh. Eksper. Teoret. Fiz. 114 (1998) 3).
[45] D.L. Nagy, L. Bottyán, L. Deák and E. Szilágyi, Balkan Phys. Lett. 5 (1997) 240.
[46] J.E. Mattson, S. Kumar, E.E. Fullerton, S.R. Lee, C.H. Sowers, M. Grimsditch, S.D. Bader and F.T. Parker, Phys. Rev. Lett. 71 (1993) 185.
[47] D.L. Nagy, L. Bottyán, L. Deák, J. Dekoster, G. Langouche, V.G. Semenov, H. Spiering and E. Szilágyi, in: *Proc. Mössbauer Spectroscopy in Materials Science*, eds. M. Miglierini and D. Petridis (Kluwer Academic, 1999) p. 323.
[48] J. Kohlhepp, M. Valkier, A. van der Graaf and F.J.A. den Broeder, Phys. Rev. B 55 (1997) 696.
[49] G.W. Anderson, P. Ma and P.R. Norton, J. Appl. Phys. 79 (1996) 5641.
[50] R.E. Vandenberghe and E. De Grave, in: *Mössbauer Spectroscopy Applied to Inorganic Chemistry*, Vol. 3, eds. G.J. Long and F. Grandjean (Plenum, New York, 1989) p. 150.
[51] P.A.A. van der Heijden, P.J.H. Bloemen, J.M. Gaines, J.T.W.M. van Eemeren, R.M. Wolf, P.J. van der Zaag and W.J.M. de Jonge, J. Magn. Magn. Mater. 159 (1996) L293.
[52] F.C. Voogt, T.T.M. Palstra, L. Niesen, O.C. Rogujanu, M.A. James and T. Hibma, Phys. Rev. B 57 (1998) R8107.
[53] L. Niesen and F.C. Voogt, unpublished (measured at ID18 at the ESRF [34]).
[54] S. Mørup and H. Topsøe, Appl. Phys. 11 (1976) 63.
[55] R. Röhlsberger, E. Gerdau, E. Lüken, H.D. Rüter, J. Metge and O. Leupold, Z. Phys. B 92 (1993) 489.
[56] T.S. Toellner, this issue, section VI-1.
[57] A. Baron, this issue, section VI-2.